

*Supporting Information for*

## **Liquid Crystal Assisted Manufacturing of Flexible Holographic Polymer Nanocomposites for High-Security Level Anticounterfeiting**

Guannan Chen,<sup>a,#</sup> Wei Wei,<sup>a,#</sup> Song Li,<sup>b,\*</sup> Xingping Zhou,<sup>a,c</sup> Zhong'an Li,<sup>a</sup> Haiyan Peng,<sup>a,c,\*</sup> Xiaolin Xie<sup>a,c</sup>

#These authors contributed equally to this work.

<sup>a</sup> Key Lab for Material Chemistry of Energy Conversion and Storage, Ministry of Education, School of Chemistry and Chemical Engineering, Huazhong University of Science and Technology (HUST), Wuhan 430074, China

<sup>b</sup> State Key Lab of Coal Combustion, School of Energy and Power Engineering, HUST, Wuhan 430074, China

<sup>c</sup> National Anti-counterfeit Engineering Research Center, HUST, Wuhan 430074, China

E-mail: songli@hust.edu.cn (S. L.), hypeng@hust.edu.cn (H. Y. P.)

## ***Supporting Characterizations***

### **(1) Nuclear magnetic resonance (NMR) spectroscopy**

<sup>1</sup>H- and <sup>13</sup>C-NMR measurements were conducted on an NMR spectrometer (400 MHz or 600 MHz, Bruker, Germany) at room temperature. Samples were dissolved in chloroform-*d* (CDCl<sub>3</sub>) for analysis and tetramethylsilane (TMS) was used as the internal standard.

### **(2) Mass spectroscopy**

Mass spectra were measured on a Fourier transform mass spectrometer (Solarix 7.0T, Bruker, Germany). Samples were dissolved in DCM (1 mg/mL) for analysis.

### **(3) Viscosity measurement**

The shear viscosity was measured at 25 °C on a rheometer (MCR 302, Anton Paar, Austria). Samples were sandwiched between two parallel circular plates (diameter: 25 mm) during the analysis. The shear rate and sample thickness were set as 0-100 s<sup>-1</sup> and 0.1 mm, respectively.

### **(4) Photopolymerization kinetics**

Photopolymerization kinetics was investigated by real-time Fourier transform infrared spectroscopy (RT-FTIR, V80, Bruker, Germany). A monochromatic 460 nm light source with an intensity of 0.6 mW/cm<sup>2</sup> was used to trigger the photoreaction. Samples were sandwiched between two parallel sodium chloride plates (sample thickness: 50 μm) and placed on a horizontal transmission apparatus during characterization. The conversion ( $\alpha$ ) of thiol (-SH) and allyl (C=C) functional groups was determined by monitoring the absorption area decrease peaked at 2570 and 3080 cm<sup>-1</sup>, respectively,<sup>1</sup>

$$\alpha = (A_0 - A_t)/A_0 \quad (\text{S1})$$

where  $A_0$  and  $A_t$  were the absorption peak areas before and after reaction, respectively.

#### **(5) Two-dimensional (2D) grazing incidence wide-angle X-ray scattering (2D-GIWAXS)**

2D-GIWAXS measurements were performed on one Xenocs-SAXS/WAXS system (France) with an X-ray wavelength of 1.34 Å. The thin film coated on glass was irradiated at a fixed angle of 0.2°. The scattering pattern was recorded by a semiconductor detector (Pilatus 1M, DECTRIS, Swiss) with an exposure time of 600 s. The distance from the sample to detector was set as 218 mm.

#### **(6) Self-diffusion coefficient measurement**

Experimental diffusion coefficients were measured on one NMR spectrometer (500 MHz, Bruker, Germany) *via* diffusion ordered spectroscopy (DOSY). At least 32 gradient increments were employed using the ledbpgp2s pulse sequence. All measurements were performed at room temperature.

*Supporting Tables:*

**Table S1.** Diffusion coefficient of thiols in each reaction system containing the LC and the diffraction efficiency of corresponding holographic gratings.

Entry	Diffusion coefficient of thiols (m <sup>2</sup> /s)	Diffraction efficiency (%)
TMP/TATATO	5.61×10 <sup>-12</sup>	0
TMP/POSS-8DB	2.85×10 <sup>-12</sup>	15±1
POSS-8SH/TATT	1.09×10 <sup>-12</sup>	0
POSS-8SH/TATATO	4.56×10 <sup>-13</sup>	94±4

**Table S2.** Refractive index of the reaction system containing 30 wt% of LC (e.g., P0616A) prior to crosslinking.

Entry	Refractive index
TMP/TATATO	1.517
POSS-8SH/TATATO	1.550

Supporting Figures:

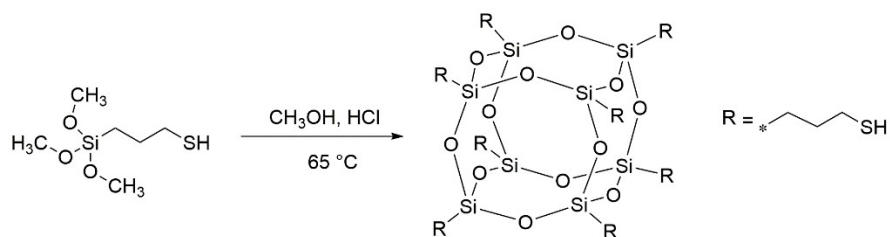


Figure S1. Synthesis of POSS-8SH.

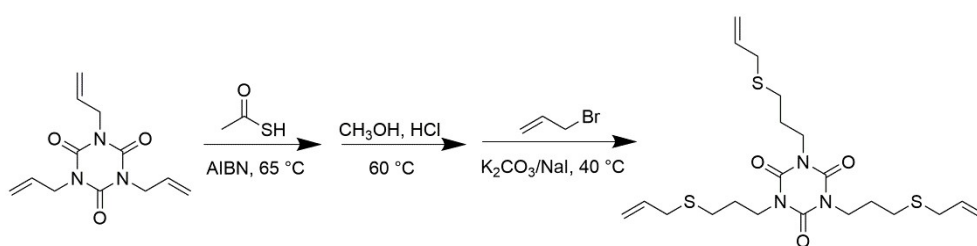


Figure S2. Synthesis of TATT.

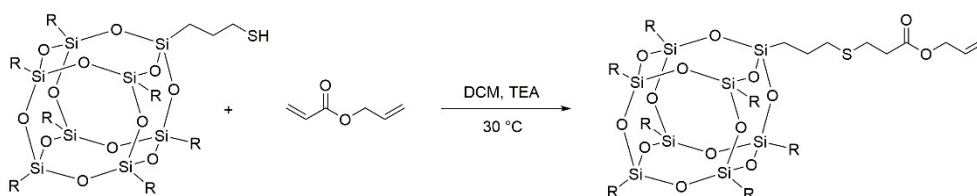
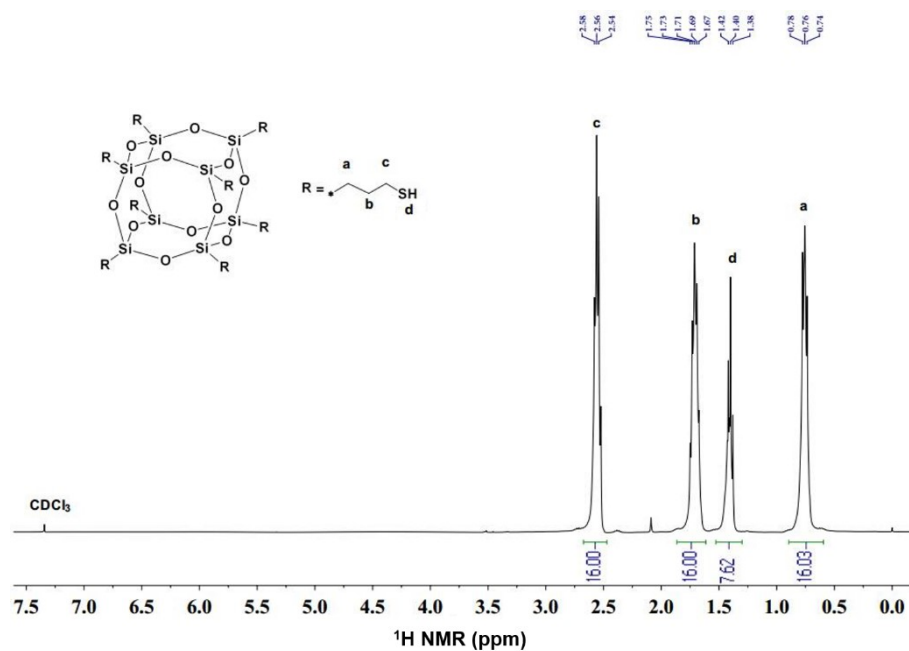
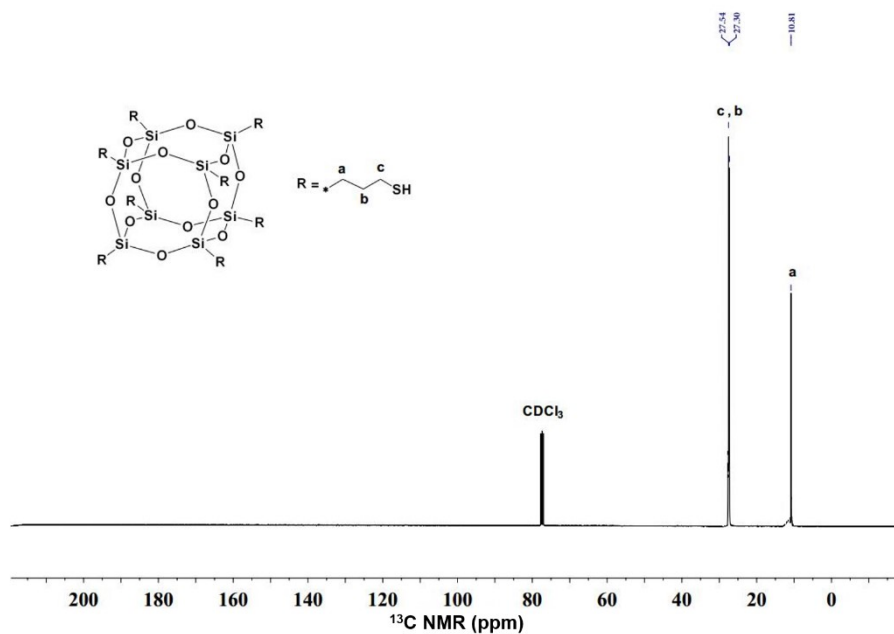


Figure S3. Synthesis of POSS-8DB.



**Figure S4.**  $^1\text{H-NMR}$  spectrum of POSS-8SH.



**Figure S5.**  $^{13}\text{C-NMR}$  spectrum of POSS-8SH.

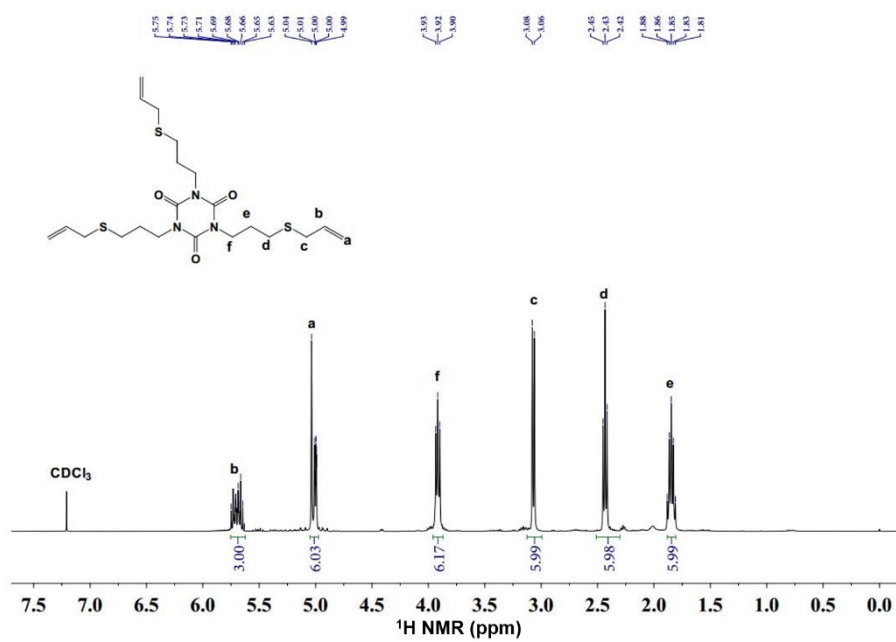


**Figure S6.**  $^1\text{H-NMR}$  spectrum of TATT.

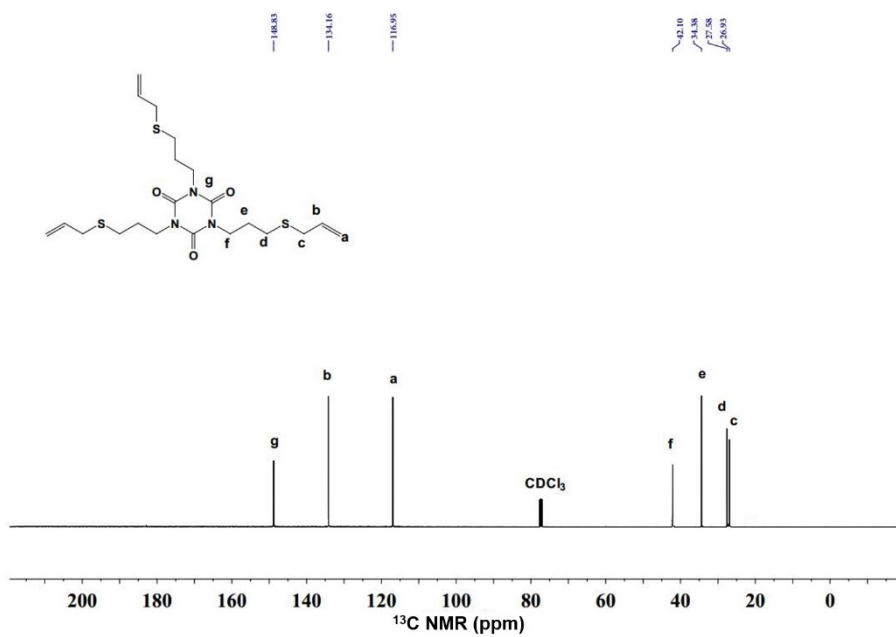


**Figure S7.**  $^{13}\text{C-NMR}$  spectrum of TATT.

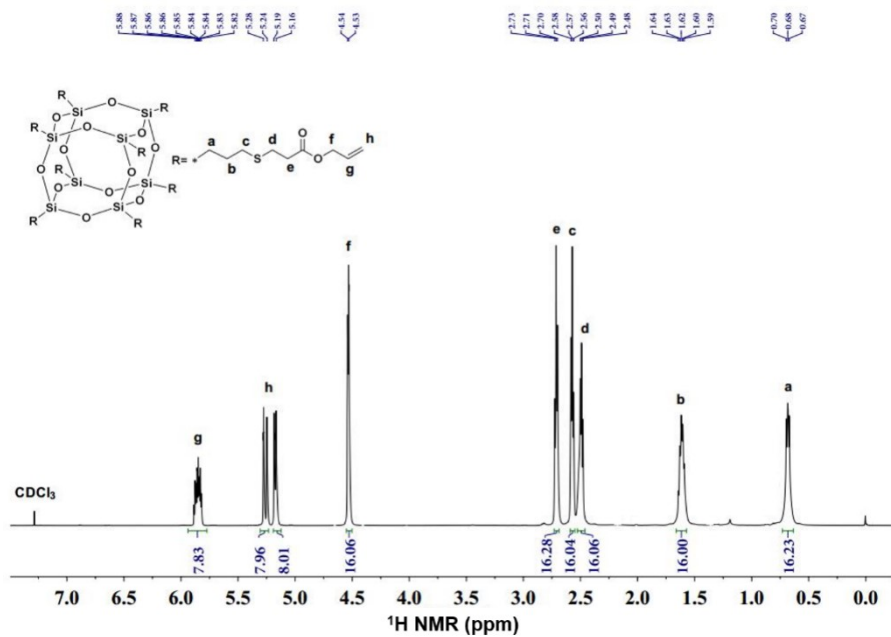


Figure S8.  $^1\text{H}$ -NMR spectrum of POSS-8DB.

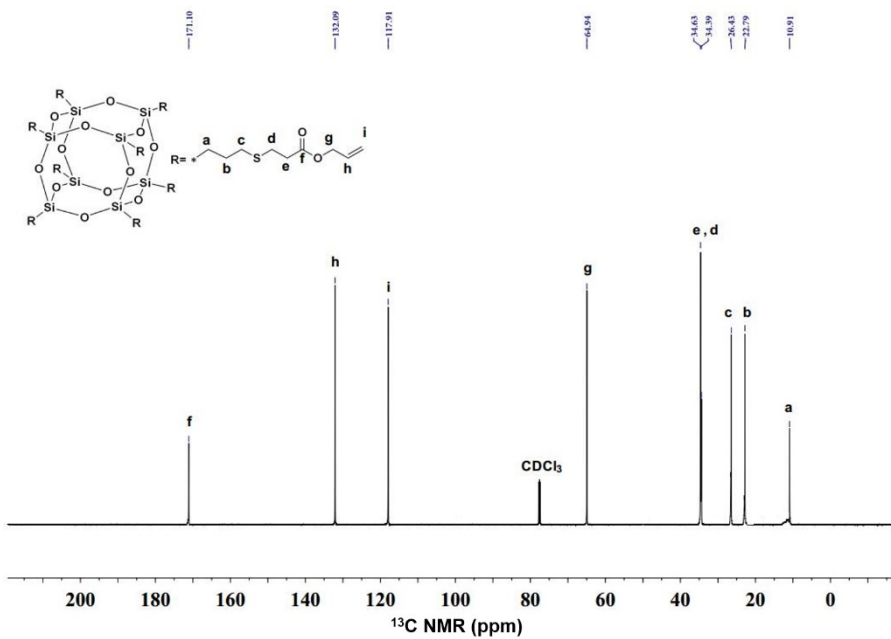
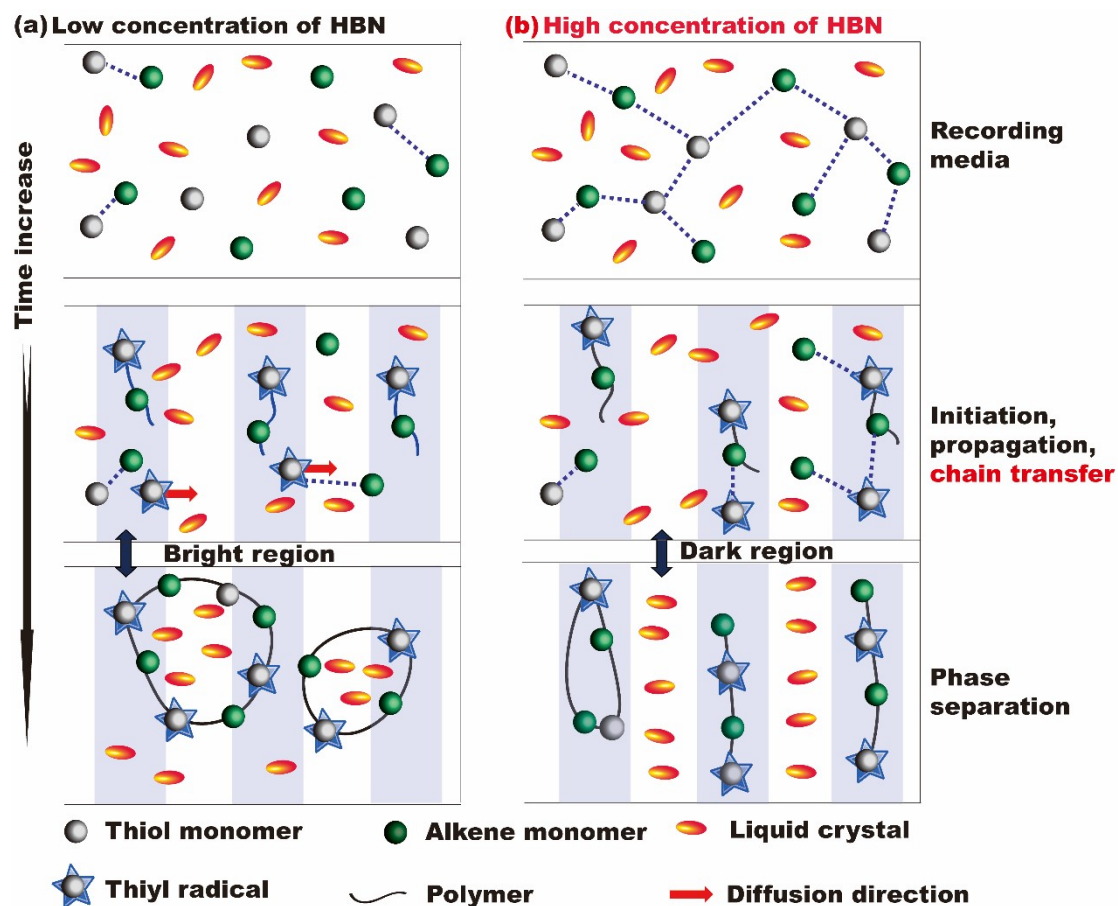
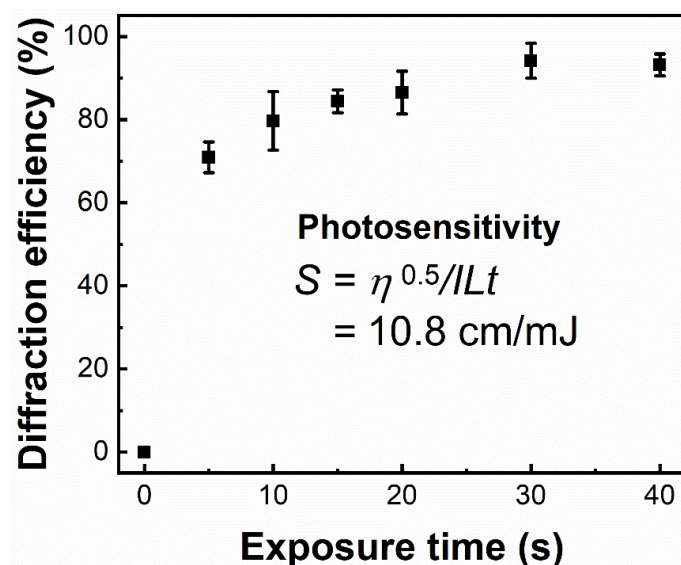


Figure S9.  $^{13}\text{C}$ -NMR spectrum of POSS-8DB.



**Figure S10.** Schematic illustration on the holographic patterning with (a) low HBN concentration, and (b) high HBN concentration. The HBN helps to constrain the diffusion of thiyl radicals from the constructive to the destructive regions upon laser interference and thus leads to well-defined phase separation.



**Figure S11.** Diffraction efficiency *versus* exposure time during holographic patterning using a two-laser interference method (laser wavelength: 460 nm, intensity: 3.0 mW/cm<sup>2</sup> for each). Photosensitivity ( $S$ ) was calculated as  $\eta^{0.5}/ILt$ , where  $\eta$  and  $L$  represented the diffraction efficiency and thickness (10  $\mu\text{m}$ ) of the reaction system.  $I$  and  $t$  were the total laser intensity and exposure time when the maximum diffraction efficiency was reached, respectively.

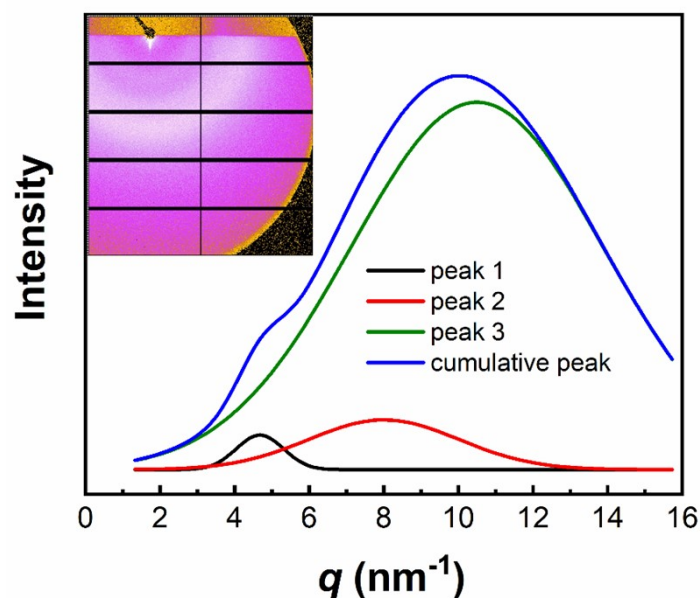


**Figure S12.** 2D-GIWAXS patterns of the holographic polymer nanocomposites containing the LC (e.g., P0616A).  $q$  represents the scattering vector. The peak 1 observed at  $q = 4.67 \text{ nm}^{-1}$  corresponds to the apparent mean nanoparticle size of POSS-8SH ( $\sim 1.34 \text{ nm}$ ). The broad peaks 2 and 3 were contributed by the LC and the LC/polythioether composite, respectively, in agreement with previous reports.<sup>2,3</sup>

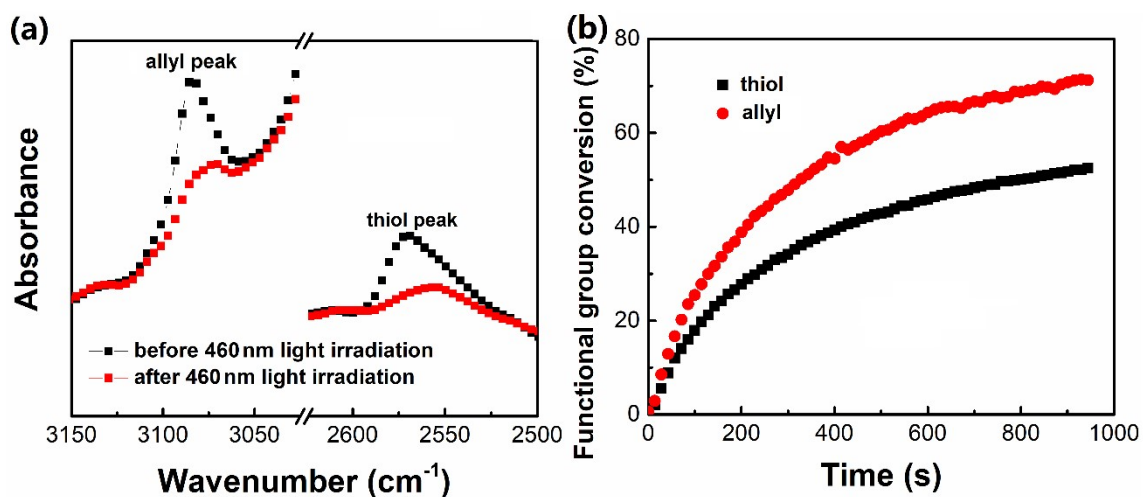


**Figure S13.** (a) Representative RT-FTIR spectra and (b) kinetics curves during the thiol-ene photoreaction upon exposure to 0.6 mW/cm<sup>2</sup> of 460 nm light. The allyl conversion is slightly higher, which is indicative of self-polymerization of some allyl monomers as reported previously.<sup>4</sup>

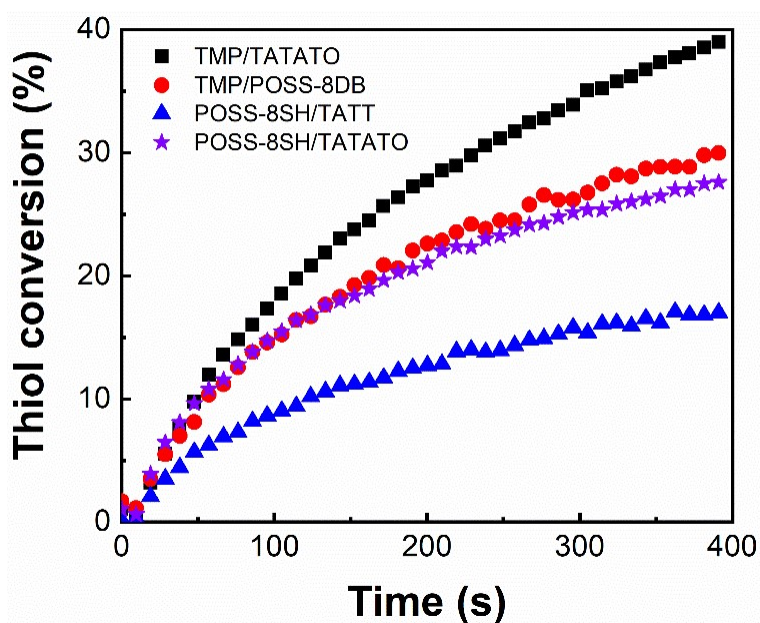


**Figure S14.** Thiol group conversion *versus* irradiation time for different systems upon exposure to 0.6 mW/cm<sup>2</sup> of 460 nm light.

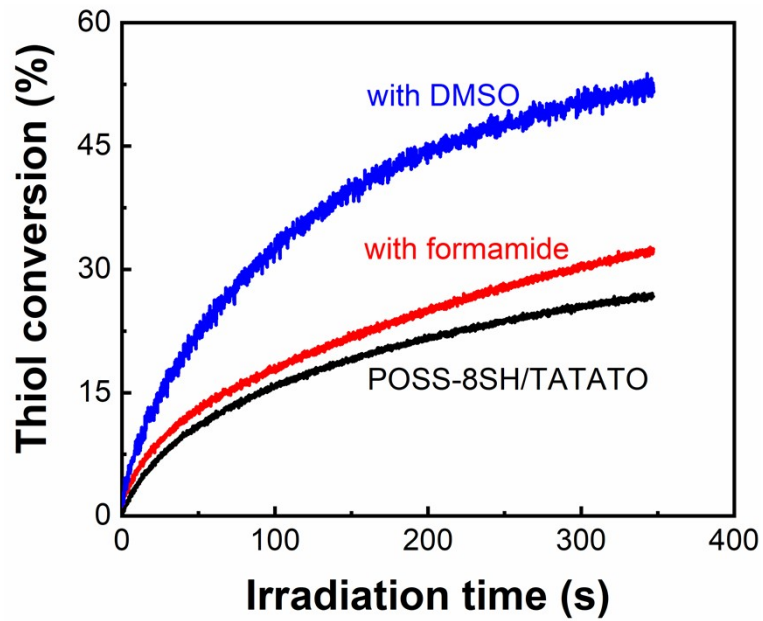


**Figure S15.** Thiol conversion against irradiation time when adding 1 wt% of formamide and DMSO in the POSS-8SH/TATATO/LC (P0616A) system.



**Figure S16.** Effect of viscosity on the coating properties on PET films.

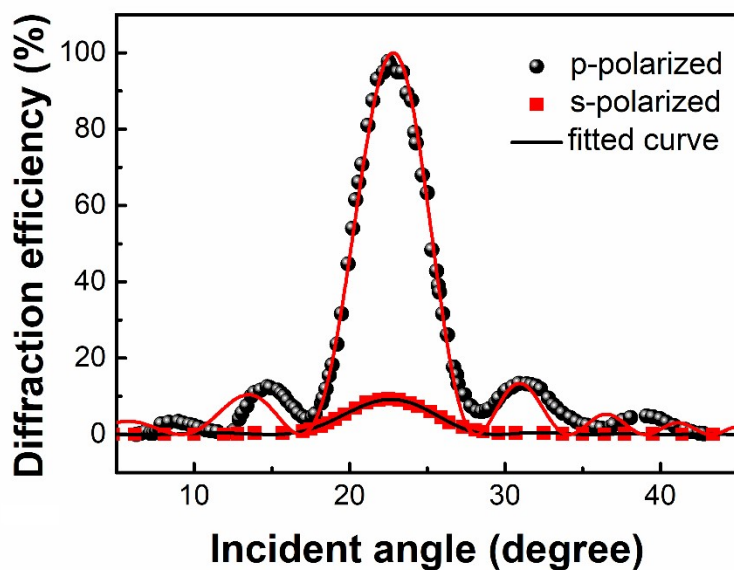


**Figure S17.** Polarization dependent diffraction efficiency of the POSS-8SH/TATATO/LC system against the incident angle of probe laser. Because of the preferential orientation of the LC molecules within the gratings, the refractive index modulation is calculated to be 0.0286 and 0.0056, respectively, for the p- and s-polarizations, according to Kogelnik's coupled wave theory.<sup>5</sup>

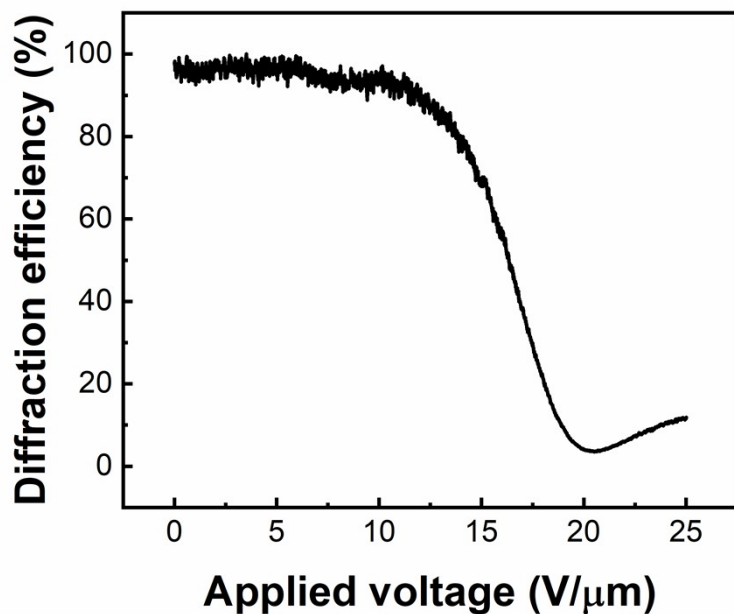


**Figure S18.** Grating diffraction efficiency *versus* applied voltage for the POSS-8SH/TATATO/LC system.

## References

1. H. Y. Peng, M. L. Ni, S. G. Bi and X. L. Xie, Photopolymerization kinetics and photo-rheological behavior of vinyl-monomers, *Acta Polym. Sin.*, 2012, **42**, 1218-1224.
2. T.-Y. Tsai, C.-Y. Lee, C.-J. Lee, W.-C. Chang, W. Lee and P.-C. Chen, Preparation and characterization of polymer-dispersed liquid crystal (PDLC) with different cation exchange capacity (CEC) clays, *J. Phys. Chem. Solids*, 2010, **71**, 595-599.
3. E. L. Heeley, D. J. Hughes, Y. El Aziz, I. Williamson, P. G. Taylor and A. R. Bassindale, Properties and self-assembled packing morphology of long alkyl-chained substituted polyhedral oligomeric silsesquioxanes (POSS) cages, *Phys. Chem. Chem. Phys.*, 2013, **15**, 5518-5529.
4. H. Y. Peng, D. P. Nair, B. A. Kowalski, W. X. Xi, T. Gong, C. Wang, M. Cole, N. B. Cramer, X. L. Xie, R. R. McLeod and C. N. Bowman, High performance graded rainbow holograms via two-stage sequential orthogonal thiol-click chemistry, *Macromolecules*, 2014, **47**, 2306-2315.
5. H. Kogelnik, Coupled wave theory for thick hologram gratings, *Bell Syst. Tech. J.*, 1969, **48**, 2909-2947.